UCRL-JC-126510
PREPRINT

LATIS Modeling of Laser Induced Midplane and Backplane Spallation

M. E. Glinsky, D. S. Bailey, and R. A. London

**This paper was prepared for submittal to
Society of Photo-Optical Instrumentation Engineers BiOS '97
San Jose, California
February 8-14, 1997**

March 5, 1997

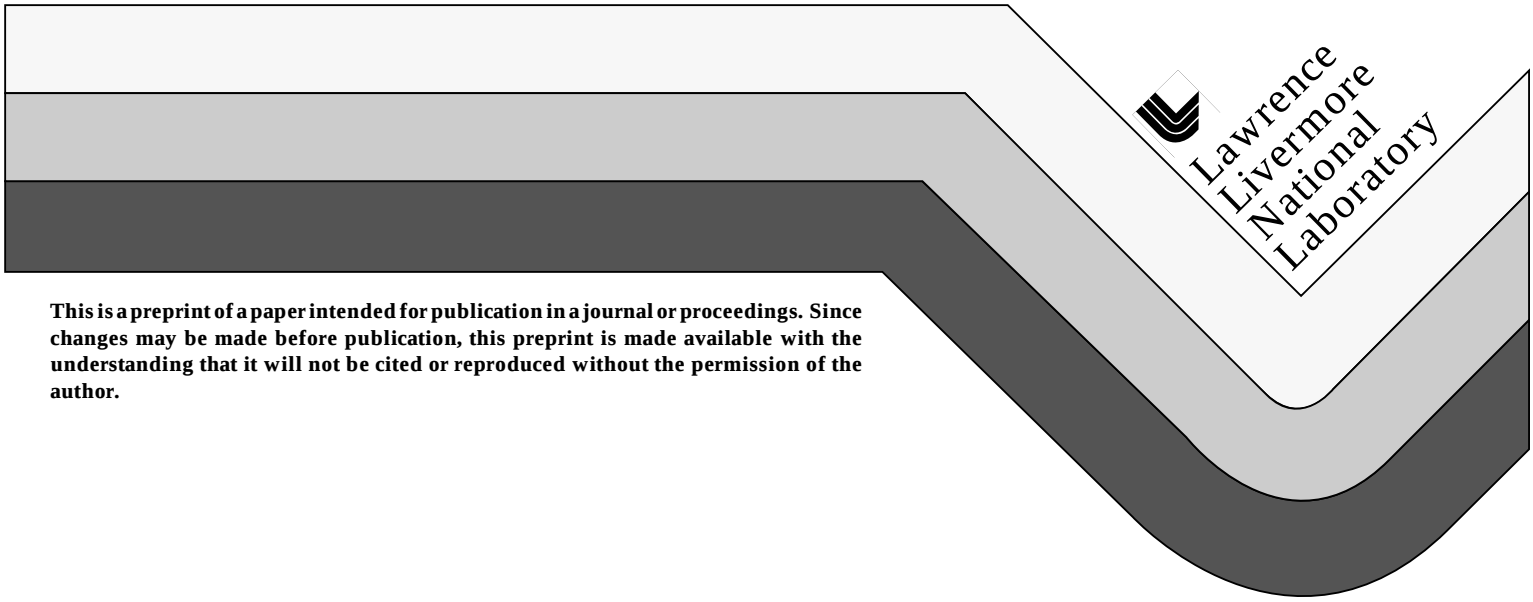

LATIS modeling of laser induced midplane and backplane spallation

Michael E. Glinsky, David S. Bailey and Richard A. London

Lawrence Livermore National Laboratory
Livermore, California 94550

ABSTRACT

The computer code LATIS is used to simulate midplane and backplane spallation resulting from short pulsed laser absorption. A 1-D planar geometry is simulated with an exponential laser absorption profile. The laser pulse length is assumed to be much shorter than the sound transit time across the laser absorption length. The boundary conditions are a fixed front plane and free backplane (backplane spall) and a free front plane and a fixed midplane (midplane spall). The NBS/NRC equation of state for water is used with a self-consistent yet empirical material strength and failure model. The failure model includes the effects of void nucleation, growth and coalescence. Definite signatures of the nucleation and coalescence thresholds are found in the back surface motion for backplane spallation.

Keywords: bubble, stress wave, material failure, acoustic radiation, simulation

2. INTRODUCTION

As the applications of laser induced stresses in medicine are being developed,[1] there is a need to know how much stress is required to damage, that is tear, biological tissue. These applications range from the cutting of eye tissue to treatments for stroke. The stress history that is required to damage the tissue, once integrated into computer simulations, can be used to design a laser induced stress that would damage or cut the unwanted tissue and not damage the nearby needed tissue. This paper will focus on experimental arrangements that can be used to measure the required thresholds for tissue damage. Simulations using hypothetical parameters for the material failure will be described, and it will be demonstrated that there are some striking qualitative differences that will delineate the needed thresholds.

The paper will be divided into three main parts. First, the basic physics of tensile material failure will be discussed. This will be used as a foundation on which the rest of the paper will be built. Second, the numerical method and the material damage model will be presented. It will be clear, when the details of this model are compared to the physics, that the model is only empirical in nature. The three basic components of the failure (nucleation, growth and coalescence) are represented in the model, but the equations used in the model are not derived in an *ab initio* way from the true physics of the failure. Third, the results of several simulations will be shown and the conclusions that one can draw from them will be stated.

The remaining part of this introduction will serve as an tutorial to the physics of tensile material failure. There are three components of material failure that must be represented in a good model of material failure. They are nucleation, growth and coalescence.[2] To see the role of each of these processes, we introduce a simulation grid on which the partial differential equations for quantities such as pressure and density are solved. We make the approximation that there are many small defects within a grid cell. These defects would be things such as dust particles in water. This approximation allows one to treat the failure in a statistical sense.

Nucleation is the birth of the element of material failure (i.e., for tensile failure of water, a bubble or void). See Fig. 1. There are two conditions that must be met for a bubble to form around a defect. First, the defect must be hydrophobic

$$\sigma_{sl} > \sigma_{gs} + \sigma_{gl}, \tag{1}$$

where σ_{sl}=energy per solid-liquid surface area, σ_{gs}=energy per gas-solid surface area, and σ_{gl}=energy per gas-liquid surface area. This allows an infinitesimal bubble to be formed around the defect without an infinite pressure being applied. Second, the pressure from surface tension $-P_{\sigma o}$ must be greater than the applied pressure

$$P < -P_{\sigma o} = -2\sigma_{gl} / R_d. \tag{2}$$

This will allow the bubble to grow. Note that the pressure threshold for nucleation of tensile failure will be determined by the largest defect size. For example, water with a failure threshold of 10 bar and a surface tension of 70 erg/cm^2 has a maximum defect size of 140 nm.

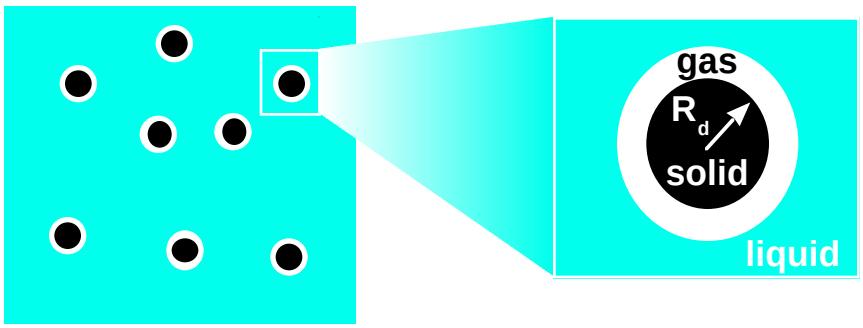

Fig. 1. Defects in a simulation cell. When defects are nucleated into bubbles a small gas layer is formed that will continue to grow into a bubble.

Once the bubble has nucleated it will grow. Its growth can be described by a Rayleigh-type equation, a second order ODE for the bubble radius R as a function of time[3]

$$\ddot{R} = f(R, \dot{R}). \tag{3}$$

This equation will have a characteristic time τ_o for the growth of the bubble from the defect size to the inter-defect spacing. The time will be a function of the applied negative pressure $\tau_o(P)$. If one assumes a characteristic pressure scale P_s for a particular set of simulations then one can use a single time $\tau_o(P_s)$.

The final stage of material failure, coalescence happens when the bubbles grow to a size that is equal to the inter-defect spacing. This is a classic problem in percolation theory.[4] If one defines the fractional bubble volume, θ_b, there will be a critical fractional bubble volume θ_{bc}. As the fractional bubble volume approaches θ_{bc} the ratio of the effective pressure applied on the bubble, P, to the average pressure applied on the simulation cell, P_o, goes to infinity (see Fig. 2). The power via which the pressure ratio goes to infinity is the critical exponent. There is a close analogy to the electrical resistivity of a block of copper with voids. The resistivity of such a structure η will be inversely proportional to the average cross sectional area of the connected volume A (see Fig. 3). As the critical point is approached the volume is broken into isolated islands, therefore the resistivity will go to infinity. Since the pressure is also inversely proportional to the average cross sectional area, it will scale the same the same way as resistivity

$$P / P_o \sim A_o / A. \tag{4}$$

The result of the large increase in the effective pressure will be to accelerate the bubble growth, thereby reducing the characteristic growth time to zero. The material will "break", no longer supporting pressure.

An *ab initio* material failure model would be based on detailed models for the nucleation, growth and coalescence of defects as described above. Such a model has not yet been fully developed. Instead, we utilize more empirical approach to material failure which represents the three components in a qualitative manner.[5]

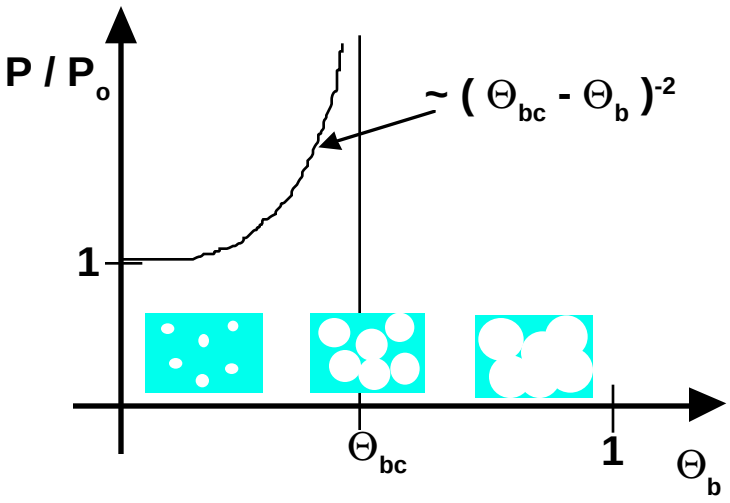

Fig. 2. Effective pressure versus fractional bubble volume.

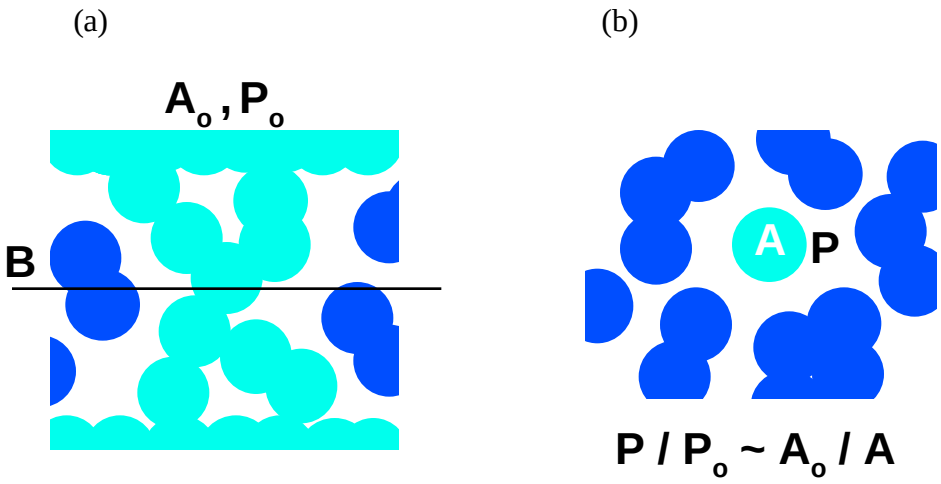

Fig. 3. Effective cross-sectional area for the support of pressure. (a) Frontal view of simulation cell. The area on the top of the cell is A_o and the average pressure is P_o. (b) A top view of the plane designated a B in Fig. 3a. The cross-sectional area of the connected volume is A and the pressure is P.

3. LATIS MODEL

Enhancements have been made to the computer code, LATIS (an acronym for LAser TISsue) developed at Lawrence Livermore National Laboratory.[6] In addition to the physics that was previously in the code (laser propagation, laser energy

deposition, hydrodynamics, atomic physics, radiation absorption, radiation emission, radiation transport, and thermal transport) we have added material strength and failure.

There are three equations that are used to advance the velocities, strains, and then the stresses in succession. The first is the dynamic equation (the fluid momentum equation) given by

$$\rho\dot{\vec{\mathrm{v}}} = -\nabla P \tag{5a}$$

where P = pressure, $\vec{\mathrm{v}}$ = velocity, and ρ = density. The second is the kinematic equation (an equation of continuity) given by

$$\dot{\theta} = \nabla \bullet \vec{\mathrm{v}} \tag{5b}$$

where θ = fractional volume change. The third is a generalization of Hooke's law given by

$$\dot{P} = -K(\dot{\theta} - \dot{\theta}_b) \ , \tag{5c}$$

where K = bulk modulus.

The values of the inelastic changes to the volume θ_b (i.e., bubble volume) are chosen such that the pressure relaxes to the minimum pressure P_σ if it is less than a minimum pressure and to zero if it is greater than zero. The inelastic change θ_b is limited so that the bubble volume, V_b, will not be less than zero nor greater than the total volume, V.

The damage index, ε_D, is calculated as

$$\varepsilon_D = \min\left(1, \frac{\theta_b}{\theta_{bc}}\right), \tag{6}$$

where θ_{bc} is the tensile strain threshold. This threshold is the critical point where the disconnected bubbles coalesce into one large one and the material "breaks". The index for tensile failure is θ_b – the maximum percentage void volume, $\max(V_b / V)$ (if the tensile damage is not allowed to heal), and V_b / V (if the tensile damage is allowed to heal). The density used to calculate the pressure is taken to be the mass in the zone divided by the volume of the cell that is not void, $V - V_b$.

The effect of the damage is to decrease the minimum pressure P_σ to $P_{\sigma o}(1 - \varepsilon_D)$. Here $P_{\sigma o}$ is the constant that characterizes the nucleation of the microscopic defects which cause material failure. This leaves one with the following expressions for the time derivatives for the inelastic volume

$$-K\,\dot{\theta}_b = \begin{cases} \dfrac{1}{\tau}[P] & \text{if } P > 0 \\ 0 & \text{if } 0 > P < P_\sigma \\ \dfrac{1}{\tau}\left[P - P_\sigma\right] & \text{if } P < P_\sigma \end{cases} \tag{7}$$

where the relaxation time is governed by the equation

$$\frac{d\tau}{dt} = \begin{cases} -\dfrac{1}{\tau_o}[\tau] & \text{if } \varepsilon_D = 1 \\ -\dfrac{1}{\tau_o}\left[\tau - \tau_o\right] & \text{if } \varepsilon_D < 1 \end{cases} \tag{8}$$

and the basic relaxation time is

$$\tau_o = \max\left(\frac{\text{zone area}}{A\, c_s \min(\Delta r, \Delta z)}, \tau_{oo}\right). \tag{9}$$

The first term is the sound transit time across the zone and prevents an instability in the numerical integration of the equations of motion. The second term is a zonal user supplied time that accounts in an empirical way for the rate dependence of the material failure. The relaxation of τ from τ_o to 0 when $\varepsilon_D = 1$ helps model the coalescence of voids. The time constant should be chosen to be the characteristic time for the disconnected flaws to grow from the size on which they are nucleated to the size of the inter-flaw spacing.

The bulk modulus used is always derived from the equation of state (EOS) tables. The EOS used in these simulations is based on the NBS steam tables. It is accurate to better than 1% in all thermodynamic quantities over the range of densities and temperatures used.[7]

4. SIMULATION RESULTS

Two sets of 1-D planar simulations were done. The geometries are shown in Figs. 4 and 5. They are meant to simplify and make uniform the stress history that a particular point experiences. The first of these is the backplane spall geometry. In this geometry, a laser beam is propagated through glass then absorbed in the material to be tested (water). Although we have shown the laser propagating from left to right, the more practical situation is to rotate the picture counter clockwise a quarter of a turn so that the glass is below the material. The material is 1 mm thick. The boundary conditions consistent with this geometry are v=0 on the left hand side and a free boundary on the right hand side. For our simulations, the laser is absorbed with an exponential profile (1/e length of 100 μm) and the energy is put into heat. The energy deposition is nearly instantaneous since the energy is added over 4 ns at a constant rate. For this case the stress confinement time is 100 ns. The initial pressure was 1 bar, the initial temperature was 17°C, and the initial density was 1 gm/cc. When the material strength and failure model is used, the tensile failure strength $P_{\sigma o}$ is set to 10 bar and the tensile failure strain θ_{bc} is set to 1%. The second configuration is the midplane spall geometry, Fig. 5.[8] In this geometry two laser beams are incident on a 2 mm thick material, one from each side. Because of the symmetry, only half of the material needs to be simulated and the velocity at the midplane will be zero. The boundary conditions used in the simulation are reversed from the backplane geometry. The left hand boundary is free and the right hand boundary is fixed, v=0.

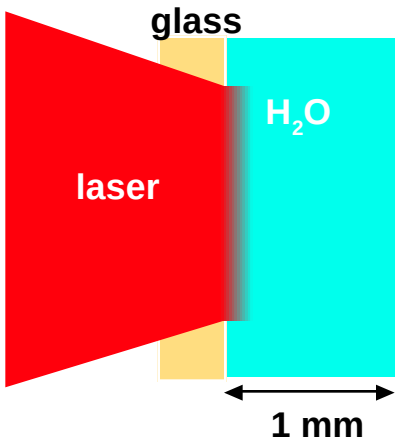

Fig. 4. Backplane spall geometry.

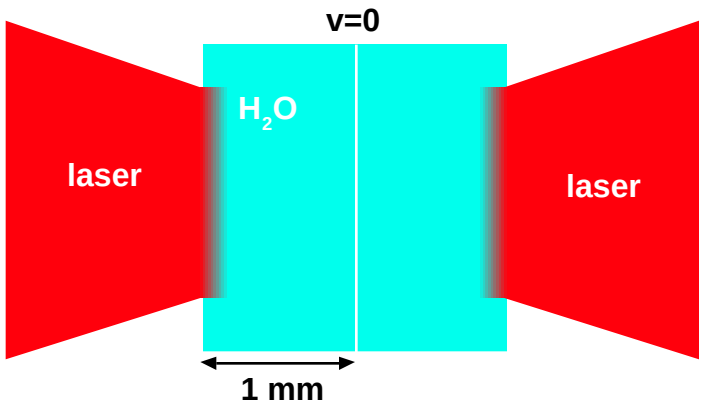

Fig. 5. Midplane spall geometry.

The results of six LATIS simulations will be shown. Three for the backplane spall geometry and three for the midplane spall geometry. The case with no material strength will be shown first. The absorbed laser energy is 0.5 J/cm^2 raising the temperature 12°C and yielding a peak pressure of 60 bar. The second case is identical to the first except the material strength and failure model is invoked. The energy absorbed is increased to 2.5 J/cm^2 for the third case and the material strength and failure model is used. The temperature rise is 58°C and the peak pressure is 600 bar.

The first simulation, Fig. 6, shows the expected result with no failure. A unipolar positive pressure pulse is launched to the right. Right after laser deposition the peak pressure is 60 bar. Half of the pressure propagates to the right forming the leading edge of the pulse. The other half propagates to the left and is reflected by the fixed boundary with no flip in polarity (the reflection coefficient is +1). This forms the trailing edge of the pulse. When the pulse reaches the right hand side of the simulation it reflects with a flip in polarity (the reflection coefficient is -1), then travels back to the left. When the pulse subsequently reflects from the left boundary it reaches its maximum tensile pressure of -60 bar.

The next simulation, Fig. 7, shows the effect of material failure. When the pulse reflects from the right hand side, the pulse is limited to the tensile failure threshold of -10 bar. When the pulse reflects from the left hand side between Fig. 7b and 7c the pressure will try to double to -20 bar as the reflected first half of the pulse overlays the second half of the pulse which is still incoming. The failure of the material limits the pressure to -10 bar which will yield a pressure pulse of only -5 bar seen in Fig. 7c. As the pulse reflects from the right hand side and becomes a compressive pulse again it recompresses the bubbles healing the failure. Although the bubbles have nucleated in this simulation they did not coalesce and were able to recompress. This is evidenced by the bubble volume. It only reaches 10-15% of the value needed for coalescence.

The third simulation, Fig. 8, has increased energy so that the bubbles can grow large enough to coalesce. This is evidenced by the bubble volume reaching 100% of the critical bubble volume between 800 and 950 μm in Fig. 8b. The 50 μm layer on the right hand side separates from the rest of the material as the density starts to drop in the failed layer and the pressure goes to zero. This spalled layer flies off ballistically at a velocity of 20 m/s. There is also some partial failure at the front surface as the -10 bar pulse reflects from the left hand side as for the previous case. This time the maximum bubble size is 40% of the value needed for coalescence. The increase is due to the greater width of the -10 bar pulse.

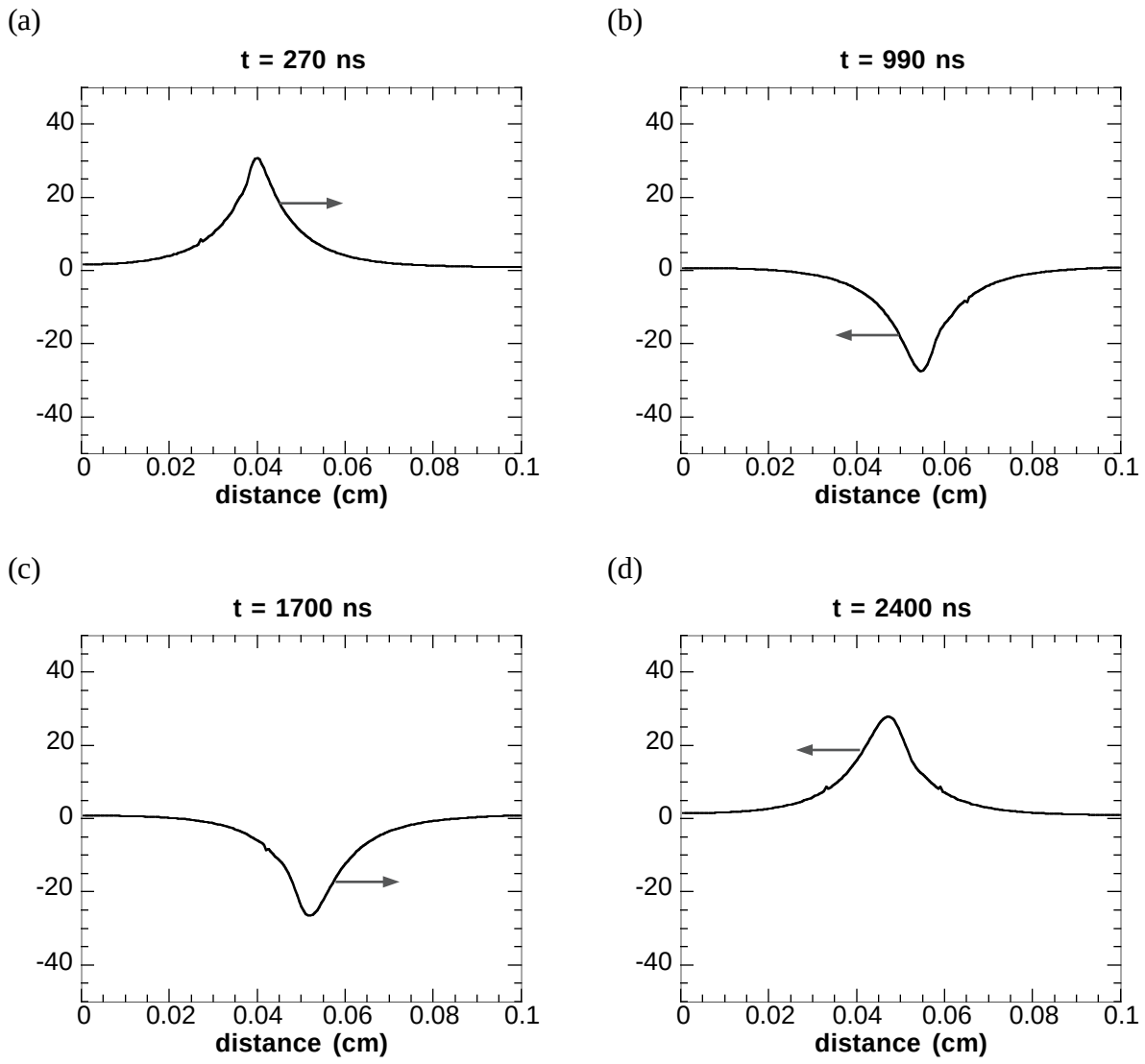

Fig. 6. Pressure (P, solid line, in bar) as a function of distance. Deposited energy=0.5 J/cm^2, $P_{\sigma o}=\infty$. Fixed surface on left, free surface on right. Backplane spallation.

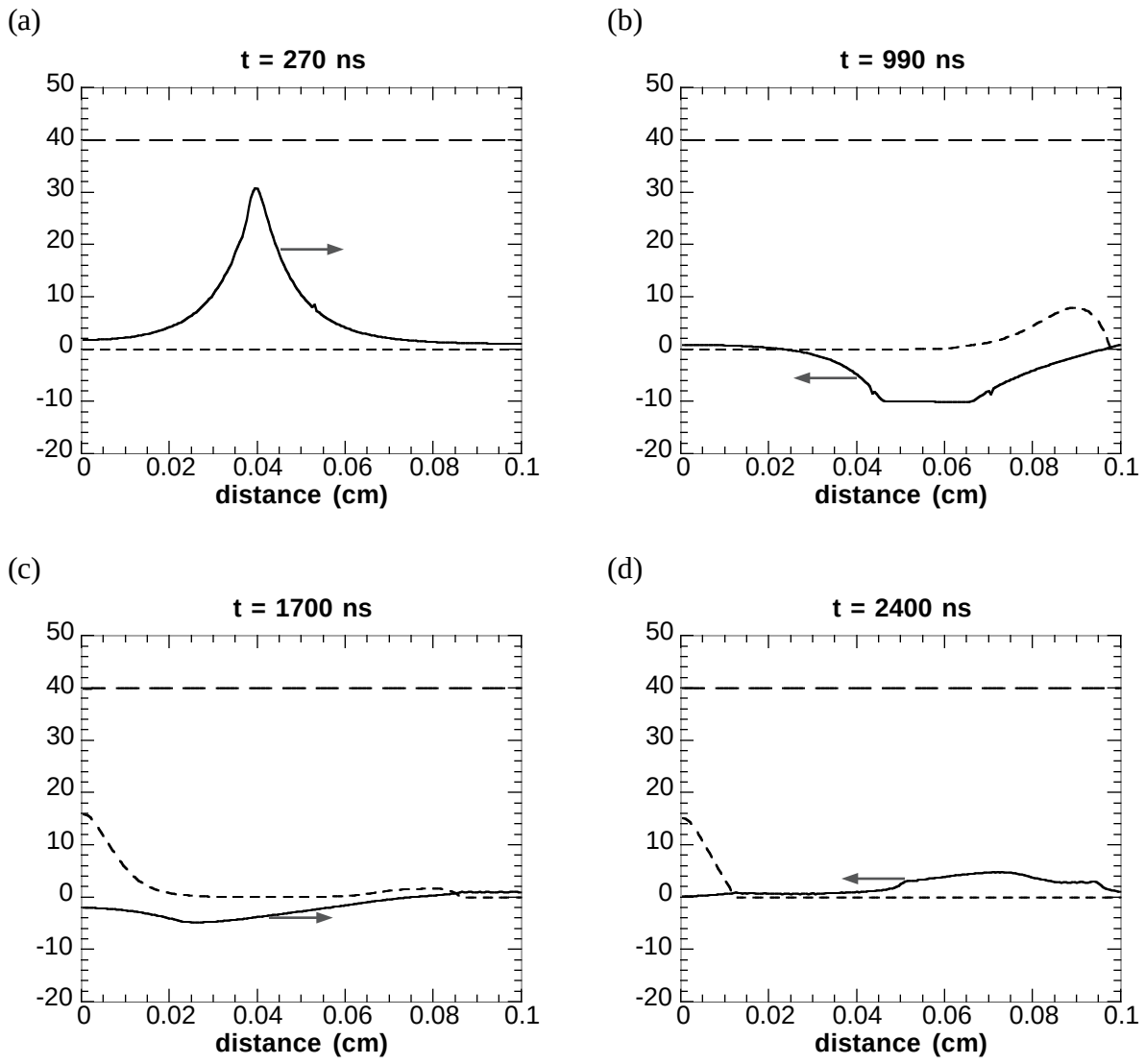

Fig. 7. Pressure (P, solid line, in bar), density (ρ, dashed line, in gm/cc multiplied by 40), normalized bubble volume (θ_b / θ_{bc}, dotted line, in %) as a function of distance. Deposited energy=0.5 J/cm^2, $P_{\sigma o}$=10 bar, θ_{bc}=1%. Fixed surface on left, free surface on right. Backplane spallation.

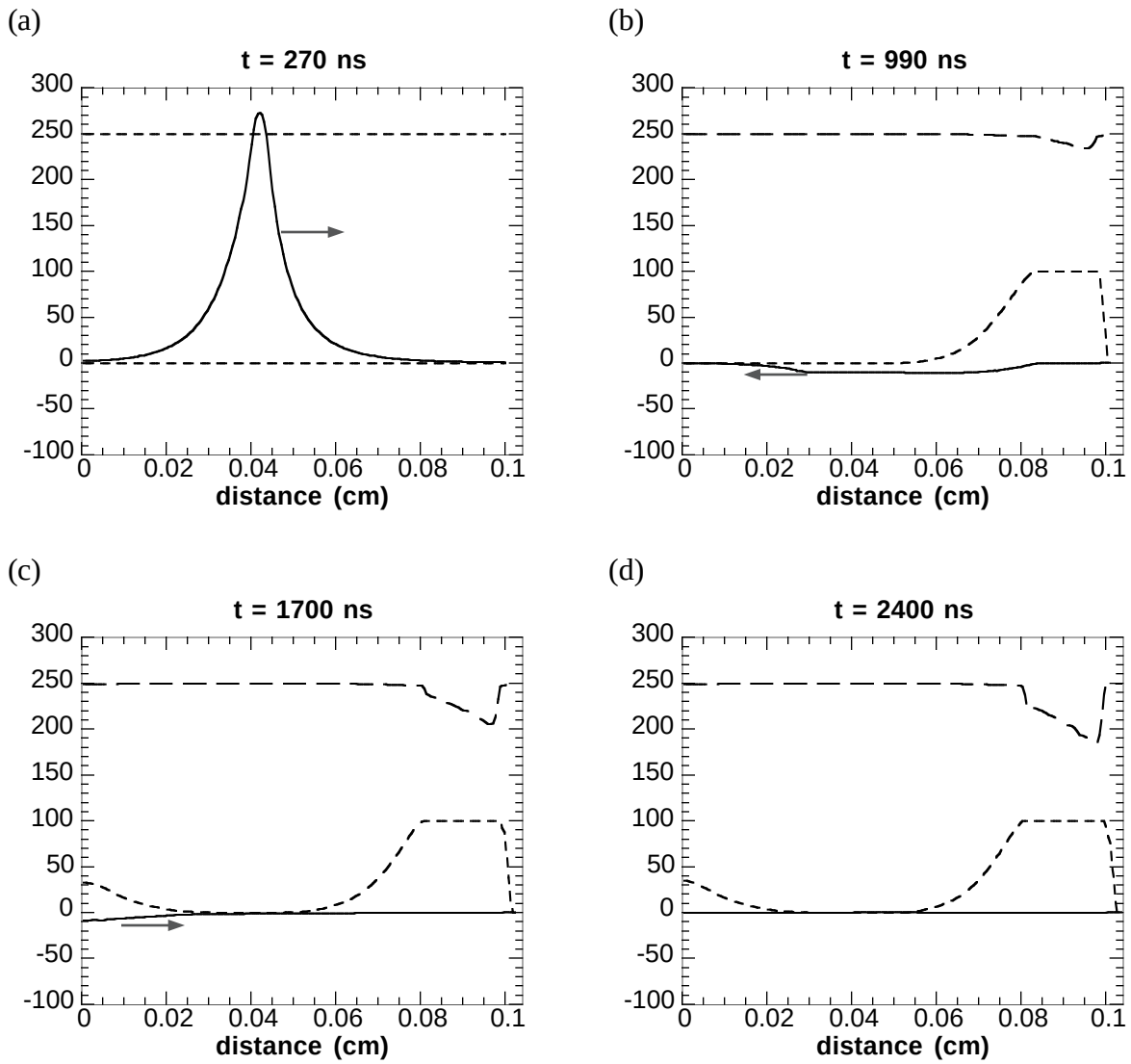

Fig. 8. Pressure (P, solid line, in bar), density (ρ, dashed line, in gm/cc multiplied by 250), normalized bubble volume (θ_b / θ_{bc}, dotted line, in %) as a function of distance. Deposited energy=2.5 J/cm^2, $P_{\sigma o}$=10 bar, θ_{bc}=1%. Fixed surface on left, free surface on right. Backplane spallation.

The next set of simulations, Figs. 9 thru 11, are analogous to the preceding three simulations except that the boundary conditions are reversed thereby giving the geometry for midplane spallation. The first of these, Fig. 9, shows what would happen if there is no material failure. The left going pressure pulse is inverted by the reflection from the free surface, yielding the bipolar pressure profile. The maximum pressure of ±60 bar is reached at the right hand boundary, that is at the midplane, between Fig. 9a and 9b.

The next simulation, Fig. 10, shows the effect of material failure. The negative part of the pressure pulse is clamped at -10 bar due to the bubble formation on the left hand side (i.e., the front surface). The maximum bubble volume near the front surface reaches only 5% of what is needed for coalescence. When the pulse reflects from the right hand side, between Fig. 10a and 10b, the negative pressure reaches -20 bar – creating bubbles at the midplane. The bubbles still can not coalesce because

the bubble volume reaches only 20% of the critical value. As the pulse approaches the left hand side, between Fig. 10b and 10c, the positive pressure causes the bubbles to collapse. When the pulse reflects off of the front, the polarity flips yielding pressures that exceed the failure threshold creating the bubbles seen in Fig. 10c. The pulse is now limited to ±10 bars as it bounces back and forth. The positive part of the pulse eventually recollapses all of the bubbles, as seen in Fig. 10d.

The final simulation, Fig. 11, shows what happens when the energy deposited is increased so that coalescence can happen. As in Fig. 10a, the negative part of the pressure pulse is clamped at -10 bar because of the formation of bubbles. In this case the bubble volume has exceeded what is needed for coalescence from 25 to 100 μm, spalling a plane off the front side that is 25 μm thick. The pulse then reflects off of the right hand side, between Figs. 11a and 11b, creating bubbles that do not quite reach the threshold for coalescence. The pressure pulse then reflects off of the plane at 100 μm, between Figs. 11b and 11c, as if it were a free surface. This creates a second zone of separation between 150 and 200 μm. A second spall plane approximately 50 μm thick is formed and moves ballistically to the left. The bubbles in the middle do not collapse, but neither do they ever coalesce.

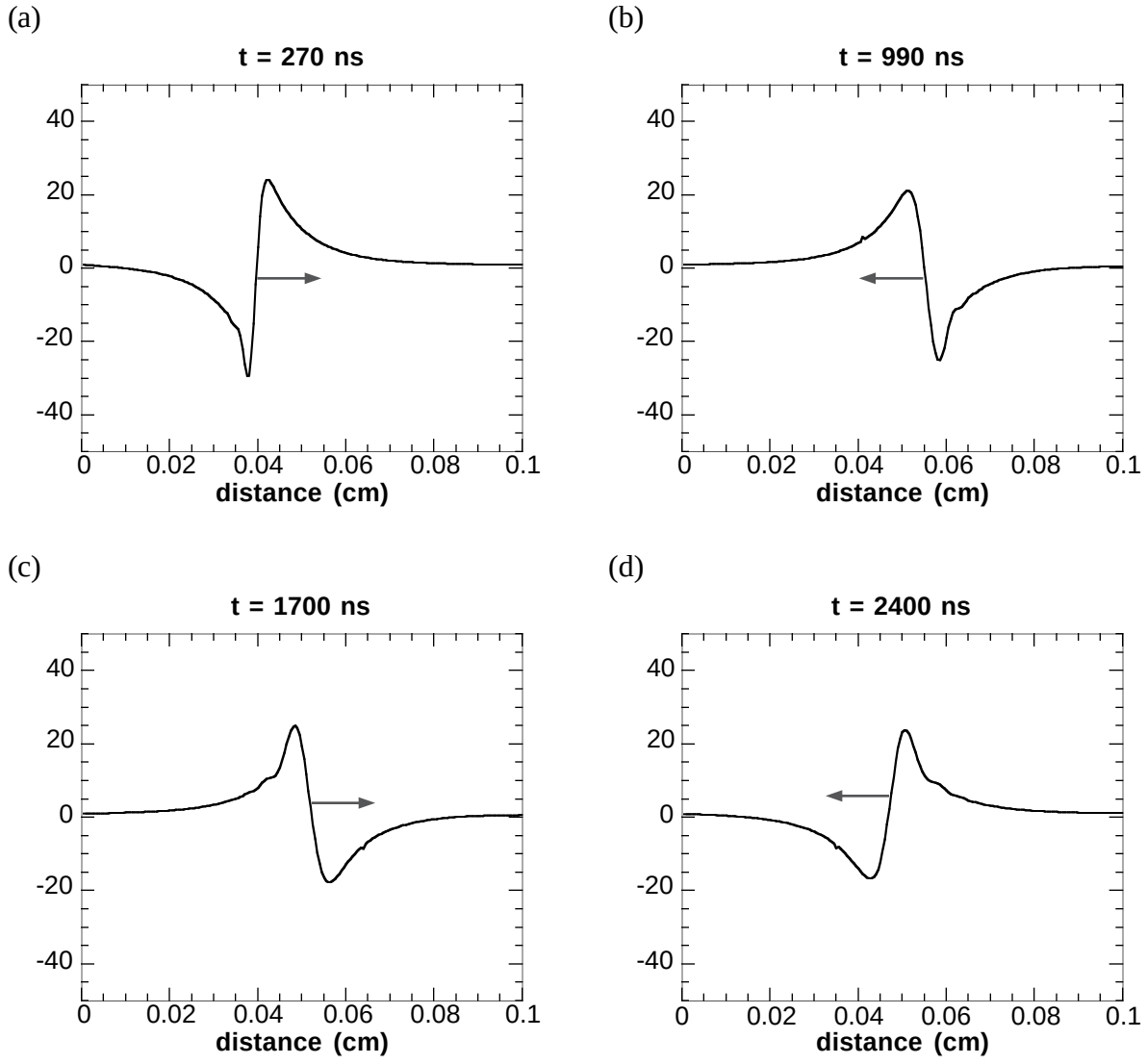

Fig. 9. Pressure (P, solid line, in bar) as a function of distance. Deposited energy=0.5 J/cm^2, $P_{\sigma 0}=\infty$. Free surface on left, fixed surface on right. Midplane spallation.

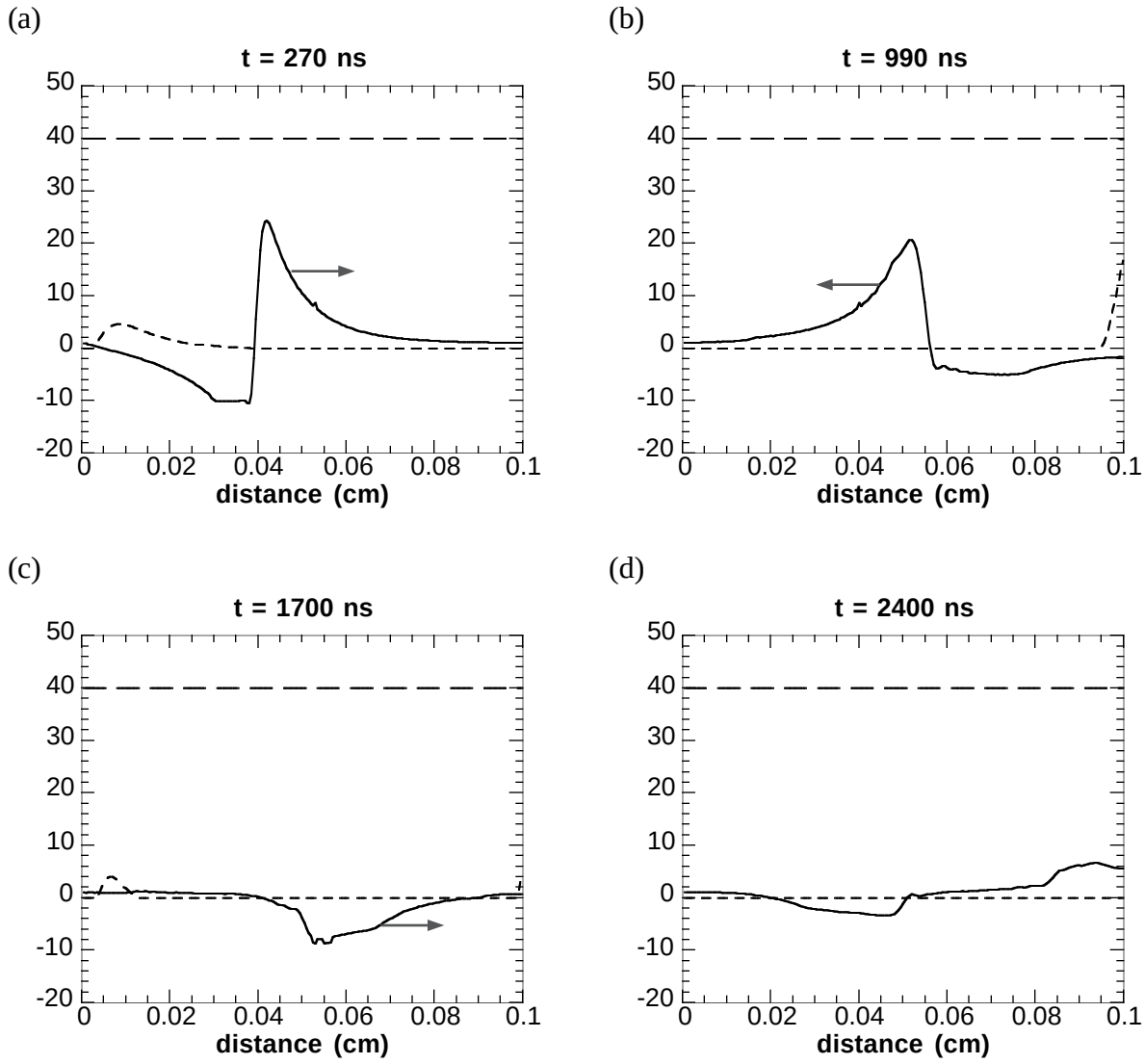

Fig. 10. Pressure (P, solid line, in bar), density (ρ, dashed line, in gm/cc multiplied by 40), normalized bubble volume (θ_b / θ_{bc}, dotted line, in %) as a function of distance. Deposited energy=0.5 J/cm^2, $P_{\sigma o}$=10 bar, θ_{bc}=1%. Free surface on left, fixed surface on right. Midplane spallation.

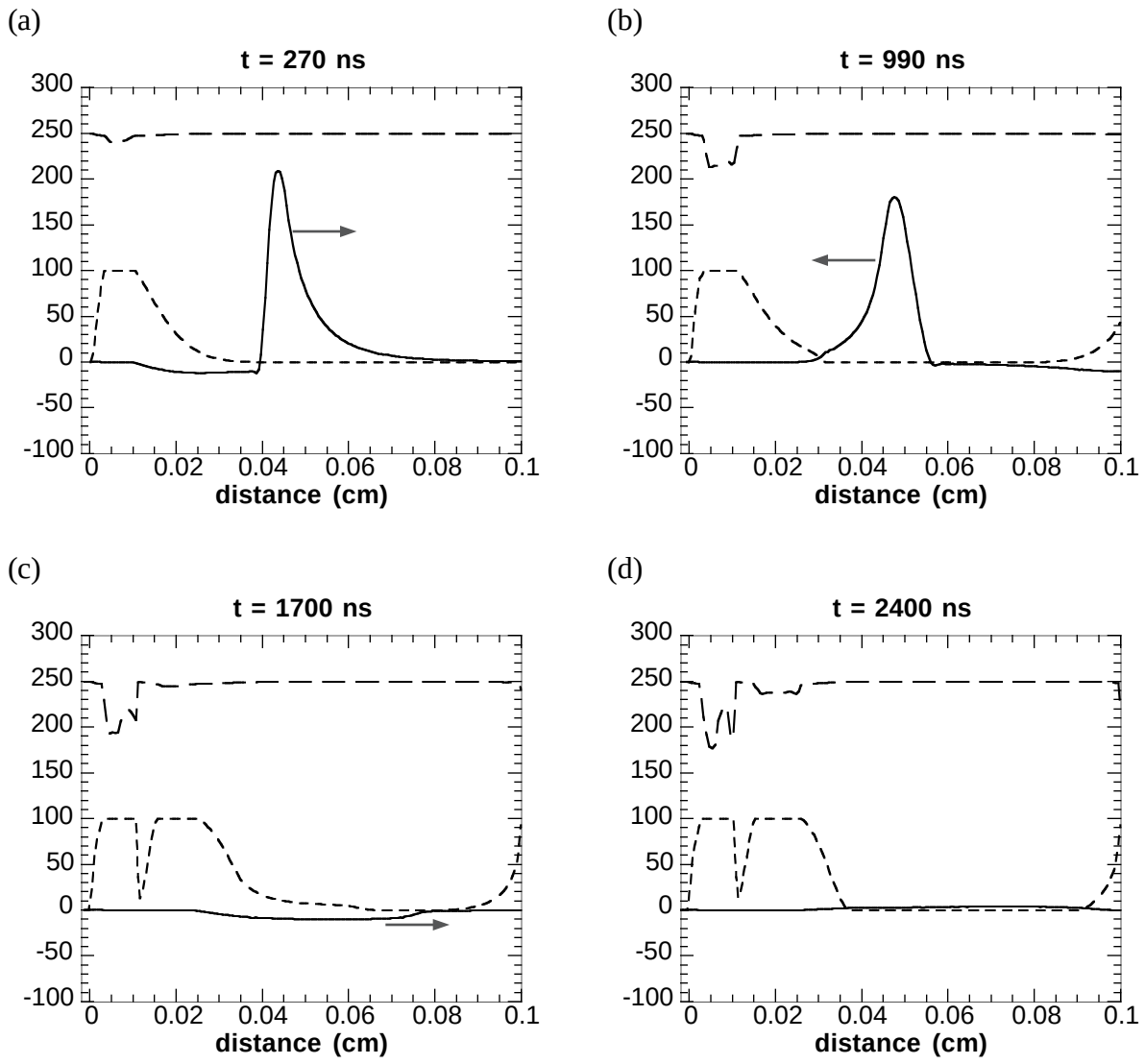

Fig. 11. Pressure (P, solid line, in bar), density (ρ, dashed line, in gm/cc multiplied by 250), normalized bubble volume (θ_b / θ_{bc}, dotted line, in %) as a function of distance. Deposited energy=2.5 J/cm^2, $P_{\sigma o}$=10 bar, θ_{bc}=1%. Free surface on left, fixed surface on right. Midplane spallation.

The final graph, Fig. 12, shows the change in the position of the backplane, that is the right hand side, for the simulations shown in Figs. 6 thru 8. It illustrates the qualitative change in behavior when the threshold for nucleation, then the threshold for coalescence is exceeded. When there is no material failure, the backplane shows a regular oscillation that returns to zero. If the threshold for nucleation is exceeded but not the threshold for coalescence, the location of the backplane stays localized but is neither displays a regular behavior nor returns to zero. Finally, when the thresholds for nucleation and coalescence are both exceeded, the backplane surface is not localized and moves away from the material with a velocity of 20 m/s.

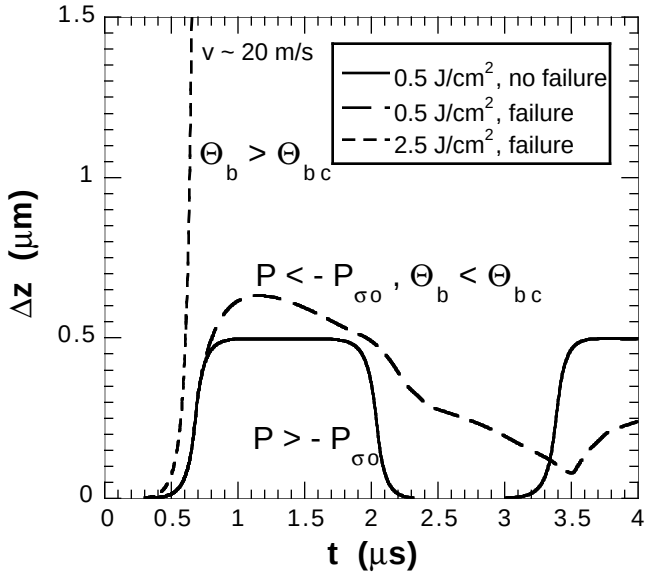

Fig. 12. Change in the location of the backplane as a function of time.

5. DISCUSSIONS AND CONCLUSIONS

The results of the LATIS simulations give insight into the stress wave propagation and resulting spall. The simple geometry of these simulations is useful for determining the parameters of the material failure. The best of the two geometries is that shown in Fig. 4 – backplane spallation. First, the material failure takes place in a region that is not heated by the laser. Such heating could lead to thermal weakening of the material that would confuse the results of the experiment. Second, the spall happens on a readily accessible surface that can be easily diagnosed with interferometry. For midplane spall, the failure first happens in the middle of the material and it never coalesces. On the front surface where there is coalescence, the incident laser complicates the measurement. Figure 12 demonstrates the utility of the back surface position measurement during backplane spall. There is a qualitative and of course quantitative way to measure both the tensile failure limit for nucleation $P_{\sigma o}$ and the failure strain for coalescence θ_{bc}. The LATIS model with material failure parameters measured via backplane spallation can be used to design medical therapies. The different design geometries and treatment protocols can be tested without constructing a physical device.

6. ACKNOWLEDGMENTS

This work was performed under the auspices of the U.S. Department of Energy by the Lawrence Livermore National Laboratory under contract W-7405-ENG-48. One of the authors (MEG) would like to acknowledge the support of a U.S. Department of Energy Distinguished Postdoctoral Fellowship. The authors acknowledge useful conversations with Steven Jacques, Alexander Oraevsky, Luiz da Silva, and Peter Celliers.

7. REFERENCES

1. K.W. Gregory, "Laser thrombolysis," *Interventional Cardiology*, E.J. Topol, editor, W.B. Sanders & Co., Vol. 2, p. 892, 1994; M. Strauss et al., "Computational modeling of laser thrombolysis for stroke treatment", *Proceedings of Lasers in Surgery: Advanced Characterization, Therapeutics, and Systems VI*, Vol. 2671, pp. 11-21, 1996; D. Palanker et al., "Electric discharge induced cavitation", *Proceedings of Laser Tissue Interaction VIII*, Vol. 2975, 1997; A. Vogel et al., "Mechanisms of intraocular photodisruption with picosecond and nanosecond laser pulses", *Lasers in Surgery and Medicine*, Vol. 15, pp. 32-43, 1994; A. Vogel et al., "Minimization of cavitation effects in pulsed laser ablation illustrated on laser angioplasty", *Appl. Physics B*, Vol. 62, pp. 173-182, 1996; A. Vogel et al., "Shock wave emission and cavitation bubble generation by picosecond and nanosecond optical breakdown in water", *J. Acoust. Soc. Am*., Vol. 100, pp. 1-18.

2. D.R. Curran, L. Seaman and D.A. Shockey, "Dynamic failure of solids", *Phys. Reports*, Vol. 147, pp. 253-388, 1987; L. Seaman, D.R. Curran, J.B. Aidun and T. Cooper, "A microstatistical model for ductile fracture with rate effects", *Nucl. Eng. and Design*, Vol. 105, pp. 35-42, 1987; D.E. Grady, "The spall strength of condensed matter", *J. Mech. Phys. Solids*, Vol 36, pp. 353-384, 1988.

3. M.E. Glinsky et al., "Rayleigh-type model of bubble evolution with material strength compared to detailed dynamic simulations", *Proceedings of Laser Tissue Interaction VIII*, Vol. 2975, 1997; Lord Rayleigh, "On the pressure developed in a liquid on the collapse of a spherical cavity", *Philos. Mag*., Vol. 34, p. 94, 1917; M. Plesset, "The dynamics of cavitation bubbles", *J. Appl. Mech*., Vol. 16, p. 277, 1949; L. Trilling, "The collapse and rebound of a gas bubble", *J. Appl. Mech*., Vol. 23, pp 14-17, 1952; R. Hickling and M.S. Plesset, "Collapse and rebound of a spherical bubble in water", *Phys. Fluids*, Vol. 7, pp 7-14, 1964; F.R. Gilmore, "The growth and collapse of a spherical bubble in a visco compressible Liquid", *Calif. Inst. of Tech. Hydrodyn. Lab. Rep. 26-4*, 1950. R.T. Knapp, J.W. Daily and F.G. Hammitt, *Cavitation*, McGraw-Hill, pp. 95-151, 1970.

4. D. Stauffer and A. Aharony, *Introduction to Percolation Theory*, second edition, Taylor & Francis, 1992; M. Sahimi, *Applications of Percolation Theory*, Taylor & Francis, 1994.

5. J.F. Schatz, "Physics of SOC and TENSOR", LLNL Technical Report, UCRL-51352, 1973.

6. M.E. Glinsky et al., "Modeling of endovascular patch welding using the computer program LATIS", *Proceedings of Laser Tissue Interaction VI*, Vol. 2391, p. 262, 1995; G.B. Zimmerman and W.L. Kruer, "Numerical Simulation of laser initiated fusion", *Controlled Fusion*, Vol. 11, p. 82, 1975; R.A. London et al., "Laser-tissue interaction modeling with LATIS", submitted to *Appl. Optics*, 1997.

7. L. Haar, J.S. Gallagher and G.S. Kell, *NBS/NRC Steam Tables*, McGraw-Hill, 1984.

8. R.O. Esenaliev and S.L. Jacques, "Transent and permanent cavitation in collagen gels by laser-induced thermoelastic pressure waves", *Proceedings of Laser Tissue Interaction VII*, Vol. 2681, pp. 185-193, 1996.